Chemical Physics Letters 492 (2010) 226–234

Contents lists available at ScienceDirect

Chemical Physics Letters

journal homepage: www.elsevier.com/locate/cplett

Infrared spectroscopic detection of the methylgermyl (H_2GeCH_3) radical and its perdeuterated counterpart in low temperature matrices

Ralf I. Kaiser [a,*], William Carrier [a], Yoshihiro Osamura [b], Refaat M. Mahfouz [c]

[a] Department of Chemistry, University of Hawai'i at Manoa, Honolulu, USA
[b] Kanagawa Institute of Technology, Atsugi, Kanagawa, Japan
[c] Department of Chemistry, King Saud University, Riyadh, Saudi Arabia

ARTICLE INFO

Article history:
Received 12 March 2010
In final form 14 April 2010
Available online 24 April 2010

ABSTRACT

The C_s symmetric methylgermyl radical, $H_2GeCH_3(X^2A')$, and its D5-isotopomer were detected via infrared spectroscopy in electron-irradiated methane – germane matrices via the ν_6 mode at 839 cm^{-1} and the ν_{12} absorption at 1406 cm^{-1}. Experiments with D4-germane – D4-methane matrices also detected absorptions from the D5-methylgermyl species upon electron exposure at 624 cm^{-1} (ν_7) and 1406 cm^{-1} (ν_3) originating from the CD_3 and GeD_2 groups of the D5-methylgermyl radical. Kinetic fits suggest that methylgermyl is formed via a unimolecular decomposition of methylgermane molecules (H_3GeCH_3), which in turn were synthesized via recombination of germyl (GeH_3) and methyl (CH_3) in the matrix.

1. Introduction

During the last decade, the chemistry of silicon- and germanium-bearing molecules has received considerable attention due to the applications to chemical vapor deposition processes (CVD) and solid state electronics like Schottky barrier diodes and laser diodes [1,2]. As members of main group IV, both silicon and germanium hold four valence electrons; they further form crystal lattices, in which substituted atoms (dopants) such as boron [3,4] and nitrogen can dramatically change the electrical properties such as applied in nitrogen-doped electric field resistors [5–7]. Typically, chemical vapor deposition techniques via the hot-wire approach utilize germane – methane mixtures or methylgermane (H_3GeCH_3) [8]. During these procedures, germanium-carbon bearing molecules like $GeXH_x$ ($x = 1–6$) were identified in the gas phase as important growth species to produce amorphous, often porous germanium-carbon films [9–11]. Here, controlling the growth-limiting steps in the synthesis of germanium-carbon bearing films needs sophisticated data on the time-dependent concentrations of carbon-germanium-bearing species in actual chemical vapor deposition processes. So far, the *in situ* characterization of gaseous species in CVD processes is conducted via time resolved threshold ionization mass spectrometry. However, despite the potential importance of radical species formed within the CVD process of methylgermane such as the methylgermyl species (H_2GeCH_3), no time resolved spectroscopic probes have been established. Here, infrared absorption might present a crucial identification tool to monitor the temporal evolution of these transient species in real time. Unfortunately, the infrared absorptions of the methylgermyl radical (H_2GeCH_3) have not been assigned to date due to experimental difficulties in synthesizing the methylgermyl radical.

How could the methylgermyl radical (H_2GeCH_3) be 'made' in the laboratory? Previously, we have utilized matrix isolation spectroscopy to synthesize unstable compounds from main group IV precursor molecules in low temperature (10 K) ices upon bombardment of these targets with high energy electrons, some of them which were reported in this journal. These comprised pure methane (CH_4), silane (SiH_4), and germane (GeH_4) ices as well as binary methane – silane mixtures. Upon interaction with energetic electrons, we were able to synthesize ethane (C_2H_6), ethyl radicals (C_2H_5), ethylene (C_2H_4), vinyl radicals (C_2H_3), and acetylene (C_2H_2) in methane ices [12], disilane (Si_2H_6), *disilyl* (*Si_2H_5*) [13], disilene (H_2SiSiH_2) and its silylsilylene (H_3SiSiH) isomer, and *disilenyl* (*H_2SiSiH*) [14] in silane matrices, digermane (Ge_2H_6), *digermyl* (*Ge_2H_5*) [15], digermene (*Ge_2H_4*), *the digermenyl radical,* (*Ge_2H_3*) [16], and, di-μ-hydrido-digermanium (Ge_2H_2) in germane ices, and methylsilane (CH_3SiH_3), methylsilyl (CH_3SiH_2) and the *silylmethyl* (*SiH_3CH_2*) *isomer* [17], *methylsilylidyne* (*$SiCH_3$*) and the *silenyl* (*H_2CSiH*) *isomer* [18], and methylenesilene (H_2CSi) in methane – silane ices. Those molecules and radicals indicated in italics were identified for the first time. Detailed kinetics studies suggest that upon electron irradiation, the group IV hydrides undergo unimolecular decomposition to form initially the methyl (CH_3), silyl (SiH_3), and germyl radicals (GeH_3). Neighboring radicals can recombine; for instance, in methane – silane matrices, a methyl radical recombines with a neighboring silyl radical to form internally excited CH_3SiH_3 molecules, which are either stabilized by the matrix

* Corresponding author.
E-mail address: ralfk@hawaii.edu (R.I. Kaiser).

0009-2614/$ - see front matter © 2010 Elsevier B.V. All rights reserved.
doi:10.1016/j.cplett.2010.04.033

or decompose to CH_3SiH_2 via hydrogen atom emission. Here, we export this concept and synthesize the methylgermyl radical (H_2GeCH_3) in germane – methane ices upon electron irradiation via recombination of germyl with methyl radicals followed by unimolecular decomposition of the internally excited methylgermane molecule (H_3GeCH_3) to yield the methylgermyl radical (H_2GeCH_3).

2. Experimental

The experiments were conducted in a contamination-free ultrahigh vacuum (UHV) chamber, which was also utilized in the identification of the monobridged (B_2H_5; C_{2v}) diboranyl radical [19]. Briefly, this setup consists of a 15 l cylindrical stainless steel chamber which can be evacuated down to 3×10^{-11} torr by a magnetically suspended turbopump backed by an oil-free scroll pump. A rotatable, two stage closed cycle helium refrigerator is attached to the lid of the machine and holds a polished silver mono crystal. This crystal is cooled to about 10 K and serves as a substrate for the ice condensate. The methane (CH_4) – germane (GeH_4) and D4-methane (CD_4) – D4-germane (GeD_4) gases were premixed at a ratio 21 mbar to 16 mbar. The ice condensation is assisted by a precision leak valve, which is connected to a gas reservoir. The leak valve rests on a linear transfer mechanism; during the actual gas condensation, the deposition system is moved 5 mm in front of the silver target. This setup guarantees a reproducible thickness of the frosts at 10 K. The germane – methane ices of thicknesses of 180 ± 30 nm and composition of 1.8 ± 0.1:1 were prepared at 11 K by depositing germane (99.99%) and methane (99.99%) as well as D4-germane (99.99%) and D4-methane (99.99%) at pressures of 1×10^{-8} torr for 22 min onto the cooled silver crystal. The infrared absorptions of the frosts can be attributed to the same fundamentals, combinations, and overtone modes as observed in neat methane [12] and germane ices [15,16] together with their deuterated analog samples investigated earlier in our group (Table 1; Fig. 1); the presence of the α, β, and γ lattice modes of germane indicates the germane-rich nature of the ices as extracted from the infrared spectra. These samples were irradiated at 10 K with 5 keV electrons generated in an electron gun at beam currents of up to 1000 nA by scanning the electron beam over an area of 3.0 ± 0.4 cm^2. Accounting for irradiation time of 60 min and the extraction efficiency of 78.8% of the electrons, this exposes the targets to 2.2×10^{16} electrons. To guarantee an identification of the reaction products in the ices on line and *in situ*, a Fourier Transform infrared

Table 1
Infrared absorptions originating from methane and germane in the germane – methane frosts prior to the irradiation at 10 K; β, and γ denote lattice modes of the germane sample.

Frequency, cm^{-1}	Assignment methane	Characterization
5981	$2\nu_3$	Overtone
5798	$\nu_1 + \nu_3$	Combination
5563	$\nu_3 + 2\nu_4$	Combination
4521	$\nu_2 + \nu_3$	Combination
4294	$\nu_3 + \nu_4$	Combination
4195	$\nu_1 + \nu_4$	Combination
4131	$\nu_2 + 2\nu_4$	Combination
3841	$3\nu_4$	Overtone
3009	ν_3	Fundamental
2903	ν_1	Fundamental
2810	$\nu_2 + \nu_4$	Combination
2586	$2\nu_4$	Overtone
1526	ν_2	Fundamental
1300	ν_4	Fundamental
	Assignment germane	
4190*	$2\nu_3$	Overtone
3000**	$\nu_2 + \nu_3$	Combination
2220	$\nu_3 + \gamma$	Combination
2113	$\nu_3 + \beta$	Combination
2093	$\nu_3 + \alpha$	Combination
1736	$\nu_2 + \nu_4 + \alpha$	Combination
1725	$\nu_2 + \nu_4$	Combination
943	$\nu_4 + \gamma$	Combination
919	ν_2	Fundamental
823	$\nu_4 + \alpha$	Combination
796	ν_4	Fundamental

* Overlap with $\nu_1 + \nu_4$ from methane.
** Overlap with ν_3 from methane.

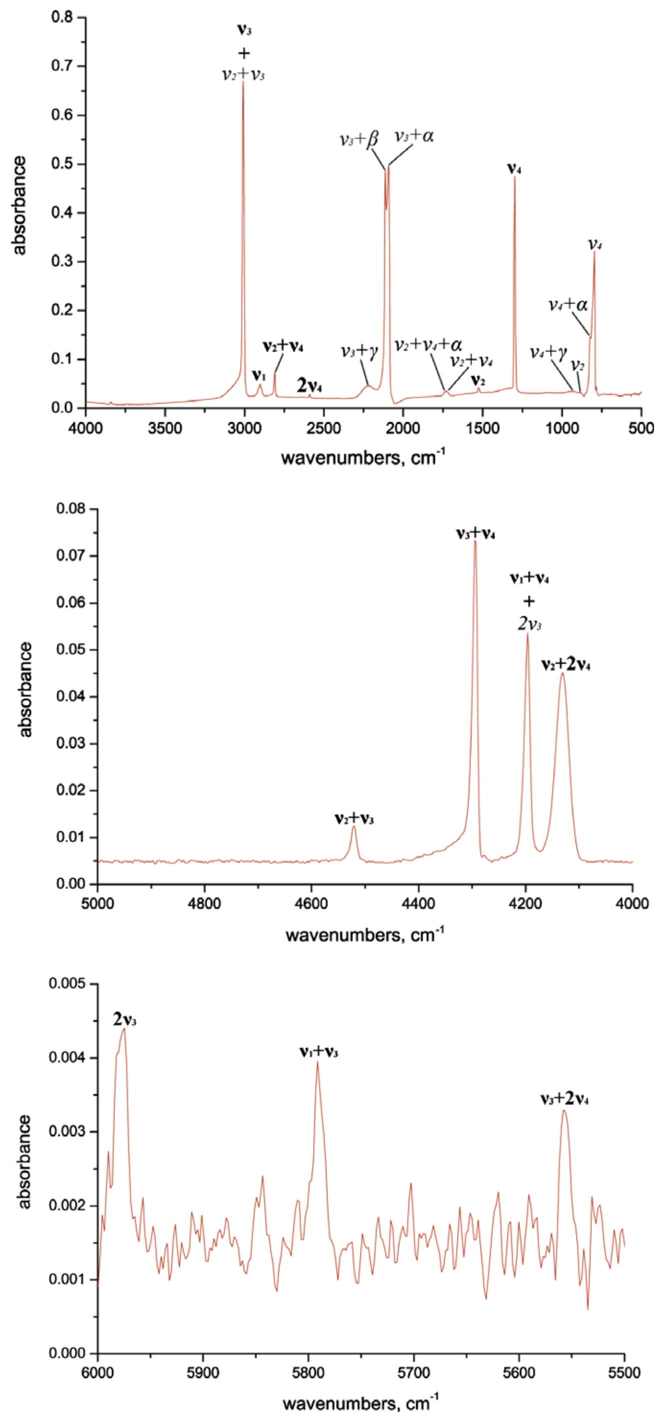

Fig. 1. Infrared spectrum of the germane – methane mixture prior to the electron irradiation at 10 K. Absorptions belonging to methane are in bold, those to germane in italics. Top: 4000–500 cm^{-1}; center: 5000–4000 cm^{-1}; bottom: 6000–5500 cm^{-1}.

spectrometer (FTIR) is utilized; spectra were averaged for 180 s at a resolution of 4 cm^{-1}.

3. Theoretical approach

We examined the molecular structures (Fig. 2) and vibrational frequencies (Table 2) of multiple isomers of the $GeCH_x$ (x = 1–6) species in terms of ab initio molecular orbital methods. The geometries were optimized with the hybrid density functional B3LYP method, i.e. Becke's three-parameter non-local exchange functional [20] with the non-local correlation functional of Lee, Yang, and Parr [21] and the 6-311G(d,p) basis set [22]. The coupled cluster CCSD(T) calculations [23,24] with the aug-cc-pVTZ basis set [25] were also performed at the optimized structures obtained with the B3LYP method in order to compare the relative energies of the isomers. All computations were carried out using the GAUSSIAN program package [26]. The relative energies stated in the text are the values obtained with the CCSD(T) method corrected with the zero-point vibrational energies obtained with the B3LYP method (Tables 3a and 3b).

4. Computational results

To identify the newly formed species carrying a germanium-carbon bond and its perdeuterated counterparts, it is important to calculate the infrared active absorptions frequencies of the $GeCH_x$ and $GeCD_x$ (x = 1–6) molecules; it is also important to compute the integrated absorption coefficients of the normal modes. These frequencies can be utilized then – after scaling – to be compared with the novel absorptions appearing in the irradiated samples. Fig. 2 depicts the structures of various $GeCH_x$ species and their structural isomers obtained with the B3LYP/6-311G(d,p) method; the energetics are compiled in Tables 3a and 3b. Considering the triatomic GeCH species, the most stable isomer is the linear GeCH radical in the doublet Π state but not in the Σ state which has triple bond between Ge and C atoms. The $^2\Sigma$ GeCH species is calculated to be 156 kJ mol^{-1} less stable than the ground $^2\Pi$ GeCH molecule. The structure of HGeC isomer is calculated to have bent structure as shown in Fig. 2 and its energy is 218 kJ mole higher than the most stable GeCH species. Three $GeCH_2$ isomers were identified, in which both hydrogen atoms were connected to the carbon ($GeCH_2$) or germanium atom (H_2GeC); in the third isomer, one hydrogen atom is linked to carbon and the second one to germanium (HGeCH). The first two isomers belong to the C_{2v} point group, whereas the HGeCH holds C_s symmetry. Since the carbon–hydrogen bond is more stable than the germanium–hydrogen bond, the thermodynamical stability of these isomers increases from H_2GeC via HGeCH to $GeCH_2$. All $GeCH_2$ isomers are in the closed-shell singlet states, and the triplet state of $GeCH_2$ is calculated to be 143 kJ mol^{-1} higher in energy than the corresponding singlet state. In the case of HGeCH isomer, the linear structure has two imaginary frequencies and the only trans form of HGeCH

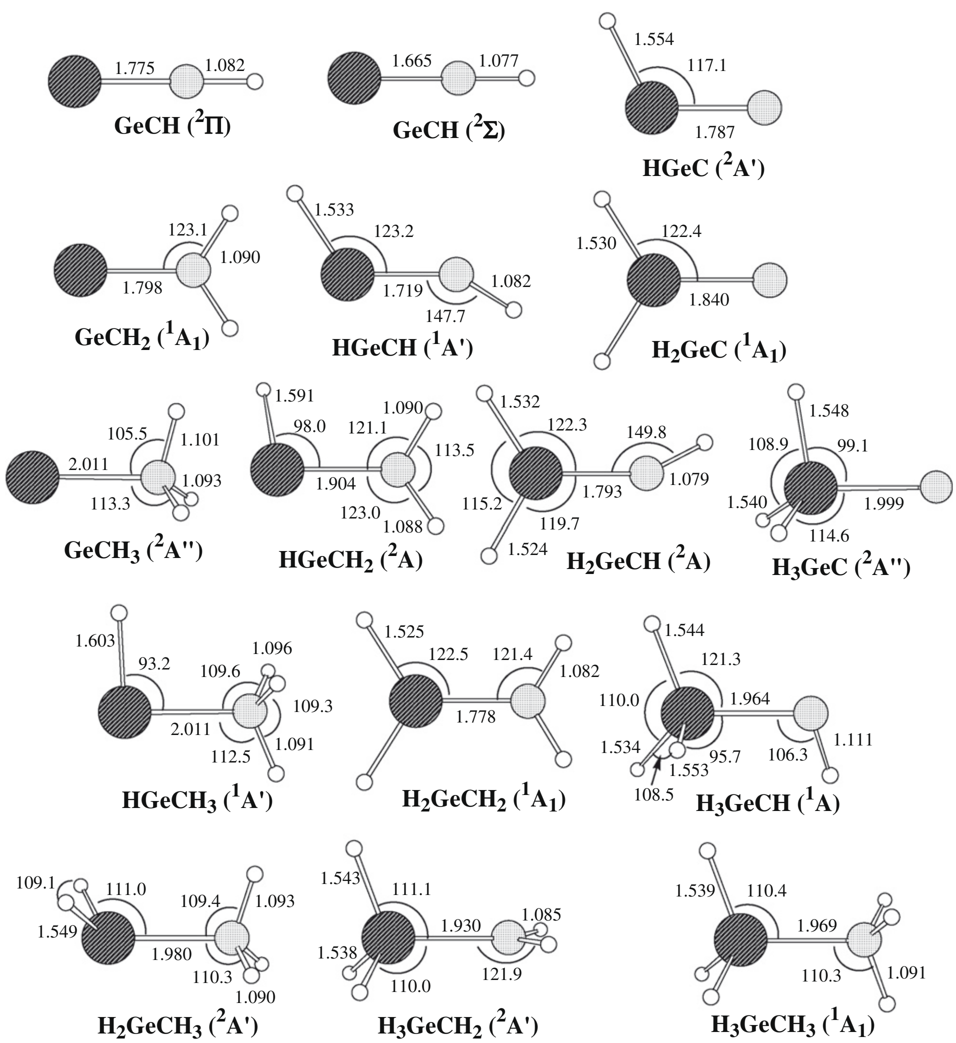

Fig. 2. Optimized structures of $GeCH_n$ (n = 1–6) species calculated with the B3LYP/6-311G(d,p) method. Bond lengths and bond angles are in Å and degrees, respectively.

Table 2
Unscaled vibrational frequencies and infrared intensities of $GeCH_n$ and $GeCD_n$ (n = 1–6) isomers calculated with the B3LYP/6-311G(d,p) method.

Mode		Frequency, cm^{-1}	Intensity, cm $molec^{-1}$	Frequency, cm^{-1}	Intensity, cm $molec^{-1}$	Characterization
		GeCH ($^2\Pi$)		**GeCD ($^2\Pi$)**		
ν_1	σ	3237	1.09E−19	2398	5.38E−19	CH stretch
ν_2	σ	865	5.59E−18	831	5.10E−18	GeC stretch
ν_3	π_x	512	2.51E−17	394	1.49E−17	Bend
ν_4	π_y	468	4.11E−18	360	2.45E−18	Bend
		GeCH ($^2\Sigma$)		**GeCD ($^2\Sigma$)**		
ν_1	σ	3284	1.78E−17	2444	9.67E−18	CH stretch
ν_2	σ	1040	6.92E−21	995	4.08E−20	GeC stretch
ν_3	π	714	7.97E−17	551	5.10E−17	Bend
		HGeC ($^2A'$)		**DGeC ($^2A'$)**		
ν_1	a'	2046	9.16E−18	1458	4.74E−18	GeH stretch
ν_2	a'	788	2.46E−20	786	4.67E−20	GeC stretch
ν_3	a'	205	6.57E−18	150	3.70E−18	Bend
		$GeCH_2$ ($^1A_1$)		**$GeCD_2$ ($^1A_1$)**		
ν_1	a_1	3083	6.07E−20	2238	4.72E−20	CH_2 sym. stretch
ν_2	a_1	1344	2.28E−18	1041	3.46E−18	CH_2 scissor
ν_3	a_1	786	3.59E−18	707	1.95E−18	GeC stretch
ν_4	b_1	688	2.26E−17	540	1.41E−17	Out of plane
ν_5	b_2	3166	5.17E−19	2348	2.89E−19	CH_2 asym. stretch
ν_6	b_2	403	4.27E−20	305	1.92E−20	CH_2 rocking
		HGeCH ($^1A'$)		**DGeCD ($^1A'$)**		
ν_1	a'	3250	3.69E−19	2406	2.53E−19	CH stretch
ν_2	a'	2097	6.06E−18	1495	3.02E−18	GeH stretch.
ν_3	a'	943	6.99E−19	895	7.42E−20	GeC stretch
ν_4	a'	775	1.44E−17	607	9.10E−18	CH bend
ν_5	a'	313	1.13E−17	226	5.99E−18	GeH bend
ν_6	a'	534	1.97E−17	398	1.15E−17	Torsion
		H_2GeC ($^1A_1$)		**D_2GeC ($^1A_1$)**		
ν_1	a_1	2105	3.46E−18	1495	1.67E−18	GeH_2 sym. stretch
ν_2	a_1	795	5.62E−19	782	1.18E−18	GeC stretch, GeH_2 scissor
ν_3	a_1	768	5.86E−18	557	2.77E−18	GeC stretch, GeH_2 scissor
ν_4	b_1	311	2.24E−19	230	2.83E−20	Out of plane
ν_5	b_2	2138	9.09E−18	1526	4.97E−18	GeH_2 asym. stretch
ν_6	b_2	219	6.80E−18	168	4.90E−18	GeH_2 rocking
		$GeCH_3$ ($^2A''$)		**$GeCD_3$ ($^2A''$)**		
ν_1	a'	3060	3.44E−18	2255	1.59E−18	CH_3 asym. stretch
ν_2	a'	2985	1.20E−18	2143	2.66E−19	CH_3 sym. stretch
ν_3	a'	1448	3.03E−18	1052	1.32E−18	CH_3 deformation
ν_4	a'	1232	1.23E−18	951	2.49E−18	CH_3 umbrella
ν_5	a'	587	3.37E−18	410	4.84E−19	CH_3 rocking
ν_6	a'	502	4.83E−18	495	6.01E−18	GeC stretch
ν_7	a'	3089	1.27E−18	2284	5.31E−19	CH_3 asym. stretch
ν_8	a'	1358	1.40E−18	975	7.99E−19	CH_3 deformation
ν_9	a'	540	1.25E−18	409	6.14E−19	CH_3 rocking
		$HGeCH_2$ (^2A)		**$DGeCD_2$ (^2A)**		
ν_1	a	3180	9.51E−19	2362	4.67E−19	CH_2 asym. stretch
ν_2	a	3084	1.78E−18	2234	8.78E−19	CH_2 sym. stretch
ν_3	a	1898	4.20E−17	1352	2.14E−17	GeH stretch
ν_4	a	1391	3.73E−19	1046	1.50E−19	CH_2 scissor
ν_5	a	815	1.07E−17	636	5.60E−18	GeH bend, CH_2 rocking
ν_6	a	684	9.99E−18	588	5.13E−18	GeC stretch
ν_7	a	571	8.74E−19	433	1.61E−18	CH_2 rocking
ν_8	a	555	3.12E−20	398	1.35E−19	Torsion
ν_9	a	436	2.54E−18	336	1.54E−18	GeH bend
		H_2GeCH (^2A)		**D_2GeCD (^2A)**		
ν_1	a	3269	6.43E−19	2417	5.87E−19	CH stretch
ν_2	a	2185	9.51E−18	1556	5.78E−18	GeH stretch
ν_3	a	2131	1.00E−17	1516	4.65E−18	GeH stretch
ν_4	a	899	1.22E−18	844	5.50E−19	GeC stretch
ν_5	a	841	6.65E−18	615	3.86E−18	GeH_2 scissor
ν_6	a	617	6.59E−18	449	3.89E−18	GeH_2 out of plane
ν_7	a	560	8.81E−18	434	6.37E−18	GeH_2 rocking
ν_8	a	384	2.82E−18	280	1.22E−18	CH bend
ν_9	a	206	4.63E−18	157	3.00E−18	Torsion
		H_3GeC ($^2A''$)		**D_3GeC ($^2A''$)**		
ν_1	a'	2111	1.37E−17	1502	8.00E−18	GeH_3 asym. stretch
ν_2	a'	2084	6.31E−18	1480	2.62E−18	GeH_3 sym. stretch

(continued on next page)

Table 2 (*continued*)

Mode		Frequency, cm^{-1}	Intensity, cm $molec^{-1}$	Frequency, cm^{-1}	Intensity, cm $molec^{-1}$	Characterization
ν_3	a'	876	7.51E−18	624	4.05E−18	GeH_3 deformation
ν_4	a'	777	1.74E−17	556	9.77E−18	GeH_3 umbrella
ν_5	a'	572	1.32E−18	570	1.10E−19	GeC stretch
ν_6	a'	288	5.99E−18	217	3.82E−18	GeH_3 rocking
ν_7	a'	2112	2.06E−17	1507	1.10E−17	GeH_3 asym. stretch
ν_8	a'	842	4.48E−18	599	2.34E−18	GeH_3 deformation
ν_9	a'	395	3.60E−18	295	2.34E−18	GeH_3 rocking
		$HGeCH_3$ ($^1A'$)		**$DGeCD_3$ ($^1A'$)**		
ν_1	a'	3117	2.76E−18	2309	1.18E−18	CH_3 asym. stretch
ν_2	a'	3006	1.05E−18	2156	2.38E−19	CH_3 sym. stretch
ν_3	a'	1859	6.31E−17	1324	3.22E−17	GeH stretch
ν_4	a'	1443	8.67E−19	1044	5.48E−19	CH_3 deformation
ν_5	a'	1239	1.35E−18	956	2.60E−18	CH_3 umbrella
ν_6	a'	890	8.75E−18	675	4.22E−18	GeH bend, CH_3 deformation
ν_7	a'	612	1.96E−18	436	6.18E−19	GeH bend
ν_8	a'	527	7.28E−18	484	6.45E−18	GeC stretch
ν_9	a''	3066	3.14E−18	2265	1.68E−18	CH_3 asym. stretch
ν_{10}	a''	1454	1.65E−18	1055	8.13E−19	CH_3 deformation
ν_{11}	a''	580	2.65E−19	430	1.79E−19	CH_3 deformation
ν_{12}	a''	128	5.13E−20	91	2.04E−20	Torsion
		H_2GeCH_2 ($^1A_1$)		**D_2GeCD_2 ($^1A_1$)**		
ν_1	a_1	3151	1.27E−19	2284	8.72E−21	CH_2 sym. stretch
ν_2	a_1	2155	4.71E−18	1530	2.57E−18	GeH_2 sym. stretch
ν_3	a_1	1394	4.30E−19	1080	5.99E−19	CH_2 scissor
ν_4	a_1	869	2.28E−18	611	3.06E−18	GeH_2 scissor
ν_5	a_1	833	4.16E−18	760	2.62E−19	GeC stretch
ν_6	a_2	718	0.00E+00	508	0.00E+00	Torsion
ν_7	b_1	748	9.06E−18	567	6.16E−18	CH_2 out of plane
ν_8	b_1	333	3.00E−18	252	1.68E−18	GeH_2 out of plane
ν_9	b_2	3255	2.21E−20	2424	6.03E−20	CH_2 asym. stretch
ν_{10}	b_2	2171	1.65E−17	1549	8.83E−18	GeH_2 asym. stretch
ν_{11}	b_2	822	9.12E−18	639	5.99E−18	CH_2 rocking
ν_{12}	b_2	457	2.29E−18	327	1.11E−18	GeH_2 rocking
		H_3GeCH (^1A)		**D_3GeCD (^1A)**		
ν_1	a	2946	8.74E−18	2163	4.06E−18	CH stretch
ν_2	a	2149	1.44E−17	1530	8.22E−18	GeH stretch
ν_3	a	2094	2.44E−17	1491	1.28E−17	GeH stretch
ν_4	a	2063	6.97E−18	1466	3.22E−18	GeH stretch
ν_5	a	896	1.35E−17	637	5.87E−18	GeH_3 deformation
ν_6	a	884	7.17E−19	667	1.47E−18	CH bend
ν_7	a	834	5.88E−18	597	2.03E−18	GeH_3 deformation
ν_8	a	789	1.31E−17	567	7.07E−18	GeH_3 umbrella
ν_9	a	600	1.31E−18	579	1.29E−18	GeC stretch
ν_{10}	a	535	9.34E−18	391	5.74E−18	GeH_3 rocking
ν_{11}	a	359	1.07E−17	273	6.61E−18	torsion
ν_{12}	a	256	1.37E−18	185	7.12E−19	GeH_3 rocking
		H_2GeCH_3 ($^2A'$)		**D_2GeCD_3 ($^2A'$)**		
ν_1	a'	3113	1.22E−18	2304	4.20E−19	CH_3 asym. stretch
ν_2	a'	3034	1.36E−18	2174	4.97E−19	CH_3 sym. stretch
ν_3	a'	2063	1.71E−17	1465	9.03E−18	GeH_2 sym. stretch
ν_4	a'	1467	7.65E−19	1062	5.82E−19	CH_3 deformation
ν_5	a'	1265	3.18E−20	977	2.82E−19	CH_3 umbrella
ν_6	a'	858	1.26E−17	604	6.28E−18	GeH_2 scissor
ν_7	a'	820	9.31E−18	632	5.43E−18	CH_3 rocking
ν_8	a'	569	1.20E−18	518	1.66E−18	GeC stretch
ν_9	a'	542	4.01E−18	391	1.54E−18	GeH_2 umbrella
ν_{10}	a''	3134	1.28E−18	2322	3.56E−19	CH_3 asym. stretch
ν_{11}	a''	2094	3.12E−17	1494	1.62E−17	GeH_2 asym. stretch
ν_{12}	a''	1459	8.48E−19	1055	7.72E−19	CH_3 deformation
ν_{13}	a''	868	5.99E−18	662	3.21E−18	CH_3 rocking
ν_{14}	a''	505	1.31E−18	359	6.25E−19	GeH_2 rocking
ν_{15}	a''	155	4.04E−20	110	1.82E−20	Torsion
		H_3GeCH_2 ($^2A'$)		**D_3GeCD_2 ($^2A'$)**		
ν_1	a'	3126	1.33E−18	2262	4.53E−19	CH_2 sym. stretch
ν_2	a'	2133	1.27E−17	1514	7.95E−18	GeH_3 sym. stretch
ν_3	a'	2099	2.03E−17	1494	9.67E−18	GeH stretch
ν_4	a'	1391	1.17E−19	1044	1.15E−20	CH_2 scissor
ν_5	a'	883	5.91E−18	630	2.77E−18	GeH_3 deformation
ν_6	a'	853	2.23E−17	615	6.92E−18	GeH_3 umbrella
ν_7	a'	634	4.57E−18	586	8.23E−18	GeC stretch
ν_8	a'	591	1.43E−17	467	9.43E−18	GeH_3 rocking, CH_2 umbrella

Table 2 (*continued*)

Mode		Frequency, cm^{-1}	Intensity, cm $molec^{-1}$	Frequency, cm^{-1}	Intensity, cm $molec^{-1}$	Characterization
v_9	a'	478	1.49E−18	347	3.34E−19	CH_2 umbrella
v_{10}	a''	3231	5.41E−19	2405	1.11E−19	CH_2 asym. stretch
v_{11}	a''	2137	2.32E−17	1524	1.24E−17	GeH_2 asym. stretch
v_{12}	a''	901	2.87E−18	646	1.02E−19	GeH_3 deformation
v_{13}	a''	804	1.01E−17	616	7.12E−18	CH_2 rocking
v_{14}	a''	501	2.10E−18	357	9.84E−19	GeH_3, CH_2 rocking
v_{15}	a''	30	2.09E−21	21	1.08E−21	Torsion
		H_3GeCH_3 ($^1A_1$)		**D_3GeCD_3 ($^1A_1$)**		
v_1	a_1	3043	1.70E−18	2182	6.05E−19	CH_3 sym. stretch
v_2	a_1	2129	1.17E−17	1509	6.28E−18	GeH_3 sym. stretch
v_3	a_1	1286	3.18E−19	997	6.22E−19	CH_3 umbrella
v_4	a_1	850	2.65E−17	610	1.40E−17	GeH_3 umbrella
v_5	a_1	586	2.95E−18	535	2.01E−18	GeC stretch
v_6	a_2	167	0.00E+00	118	0.00E+00	Torsion
v_7	e	3124	3.38E−18	2314	9.80E−19	CH_3 asym. stretch
v_8	e	2131	5.05E−17	1519	2.68E−17	GeH_3 asym. stretch
v_9	e	1473	1.12E−18	1064	1.20E−18	CH_3 deformation
v_{10}	e	908	1.81E−18	633	1.20E−17	GeH_3 deformation
v_{11}	e	857	2.63E−17	670	3.40E−18	CH_3 rocking
v_{12}	e	499	4.98E−18	356	2.32E−18	GeH_3 rocking

Table 3a
Relative energies (kJ mol^{-1}) of the isomers of each $GeCH_n$ (n = 1–5) species calculated with the CCSD(T)/aug-cc-pVTZ and B3LYP/6-311G(d,p) methods.

Species	CCSD(T)	B3LYP
GeCH ($^2\Pi$)	0	0
GeCH ($^2\Sigma$)	156	194
HGeC ($^2A'$)	218	247
$GeCH_2$ ($^1A_1$)	0	0
HGeCH ($^1A'$)	162	197
H_2GeC ($^1A_1$)	370	400
$GeCH_3$ ($^2A''$)	0	0
$HGeCH_2$ (^2A)	93	97
H_2GeCH (^2A)	191	226
H_3GeC ($^2A''$)	390	424
$HGeCH_3$ ($^1A'$)	0	0
H_2GeCH_2 ($^1A_1$)	29	59
H_3GeCH (^1A)	309	342
H_2GeCH_3 ($^2A'$)	0	0
H_3GeCH_2 ($^2A'$)	60	69

was obtained by geometry optimization. The same trend is observable within the $GeCH_3$ isomers. Here, four local minima were computed; the thermodynamical stability rises as the numbers of carbon-hydrogen bonds increase from H_3GeC via H_2GeH and $HGeH_2$ to $GeCH_3$. The next series comprises the $GeCH_4$ isomers with its members $HGeCH_3$, H_2GeCH_2, and H_3GeCH. Finally, the H_2GeCH_3, H_3GeCH_2, and H_3GeCH_3 molecules were identified as local minima. In the case of $GeCH_3$ species, the lengths of Ge–C bonds are calculated to be quite large; 2.0 Å for $GeCH_3$ and H_3GeC, and these bond distances are slightly larger than the single bond length 1.97 Å of Ge–C bond in H_3GeCH_3 molecule. While the Ge–C bond in H_2GeCH isomer (1.79 Å) seems to have double bond character, the Ge–C bond in $HGeCH_2$ isomer (1.90 Å) is weaker than that of H_2GeCH isomer. Since the optimized structure of $HGeCH_2$ does not have molecular symmetry and the CH_2 group is not in plane, $HGeCH_2$ molecule has less Π-bonding character than H_2GeCH isomer although $HGeCH_2$ is energetically more stable than H_2GeCH. Note that ethylene-type H_2GeCH_2 species and germylene $HGeCH_3$ isomers are energetically close in the case of $GeCH_4$ species. The triplet state of $HGeCH_3$ species is calculated to be 107 kJ mol^{-1} higher in energy than the singlet ground state of $HGeCH_3$ molecule.

Table 3b
Bond dissociation energies (kJ mol^{-1}) of the $GeCH_n$ (n = 1–5) species calculated with the CCSD(T)/aug-cc-pVTZ and B3LYP/6-311G(d,p) methods.

Species	Products	CCSD(T)[a]	B3LYP[a]
GeCH ($^2\Pi$)	Ge(^3P) + CH ($^2\Pi$)	464	457
	GeC ($^3\Pi$) + H (^2S)	–[b]	436
HGeC ($^2A'$)	H (^2S) + GeC ($^3\Pi$)	–[b]	190
	HGe ($^2\Pi$) + C (^3P)	297	267
$GeCH_2$ ($^1A_1$)	GeCH ($^2\Pi$) + H (^2S)	406	400
	Ge (^3P) + CH_2 ($^3B_1$)	459	437
HGeCH($^1A'$)	H (^2S) + GeCH ($^2\Pi$)	244	202
	HGe ($^2\Pi$) + CH ($^2\Pi$)	431	381
H_2GeC ($^1A_1$)	H (^2S) + HGeC ($^2A'$)	254	246
	H_2Ge ($^3B_1$) + C (^3P)	351	337
$GeCH_3$ ($^2A''$)	$GeCH_2$ ($^1A_1$) + H (^2S)	250	262
	Ge (^3P) + CH_3 ($^2A''_2$)	260	241
$HGeCH_2$ (^2A)	H (^2S) + $GeCH_2$ ($^1A_1$)	157	166
	HGe ($^2\Pi$) + CH_2 ($^3B_1$)	339	325
	HGeCH ($^1A'$) + H (^2S)	414	413
H_2GeCH (^2A)	H (^2S) + HGeCH ($^1A'$)	317	283
	H_2Ge ($^1A_1$) + CH ($^2\Pi$)	357	327
	H_2GeC ($^3A''$) + H (^2S)	456	443
H_3GeC ($^2A''$)	H (^2S) + H_2GeC ($^1A_1$)	257	245
	GeH_3 ($^2A_1$) + C (^3P)	229	227
$HGeCH_3$ ($^1A'$)	H (^2S) + $GeCH_3$ ($^2A''$)	294	285
	GeH ($^2\Pi$) + CH_3 ($^2A''_2$)	277	248
	$HGeCH_2$ (^2A) + H (^2S)	388	381
H_2GeCH_2 ($^1A_1$)	H (^2S) + $HGeCH_2$ (^2A)	358	322
	GeH_2 ($^1A_1$) + CH_2 ($^1A_1$)	440	411
	H_2GeCH (^2A) + H (^2S)	456	452
H_3GeCH ($^3A''$)	H (^2S) + H_2GeCH (^2A)	244	240
	GeH_3 ($^2A_1$) + CH ($^2\Pi$)	345	329
	H_3GeC ($^2A''$) + H (^2S)	444	437
H_2GeCH_3 ($^2A'$)	$HGeCH_3$ ($^1A'$) + H (^2S)	249	231
	H_2GeCH_2 ($^1A_1$) + H (^2S)	278	290
	GeH_2 ($^1A_1$) + CH_3 ($^2A''_2$)	230	191
H_3GeCH_2 ($^2A'$)	H (^2S) + H_2GeCH_2 ($^1A_1$)	218	221
	GeH_3 ($^2A_1$) + CH_2 ($^3B_1$)	363	344
	H_3GeCH ($^3A''$) + H (^2S)	429	434
H_3GeCH_3 ($^1A_1$)	H_2GeCH_3 ($^2A'$) + H (^2S)	358	345
	H_3GeCH_2 ($^2A'$) + H (^2S)	418	414

[a] Zero-point vibrational energies are corrected by the values calculated with B3LYP/6-311G(d,p) method.
[b] Since there is convergence problem for the CCSD(T) calculation of triplet state of GeC molecule, the dissociation energy leading to GeC species cannot be evaluated with the CCSD(T) method.

The bond distances of Ge–C are clearly demonstrated to be single bond for $HGeCH_3$ and double bond for H_2GeCH_2. The less stable H_3GeCH isomer is methylene-type structure and the geometry of the singlet state shown in Fig. 2 does not have any molecular symmetry. The relative energy of this singlet state was calculated to be 309 kJ mol^{-1} higher than the most stable $HGeCH_3$ species. The ground state of H_3GeCH species is not the singlet state and the triplet state is calculated to be 68 kJ $mole^{-1}$ more stable than the singlet state. In the case of $GeCH_5$ species, the energy difference between the most stable methylgermyl radical H_2GeCH_3 and less stable germylmethyl radical H_3GeCH_2 is only 60 kJ mol^{-1}. The bond distances of Ge–C are shown to be single bonds both in H_2GeCH_3 and H_3GeCH_2 species. We have found that the internal rotations of CH_3 and GeH_3 groups are almost free in H_3GeCH_2, H_2GeCH_3, and H_3GeCH_3 molecules.

5. Experimental results

Upon the electron irradiation of the methane – germane ices, prominent absorptions arose from those species observed previously in pure methane [12] and germane ices [15,16] such as acetylene (C_2H_2: 736 cm^{-1}, ν_5), ethylene (C_2H_4: 1435 cm^{-1}, ν_{12}), and ethane (C_2H_6: 2976 cm^{-1}, ν_1/ν_{10}; 2937 cm^{-1}, $\nu_1 + \nu_{10}$, 1371 cm^{-1}, ν_6) as well as digermane (Ge_2H_6: 871 cm^{-1}, ν_{11}; 758 cm^{-1}, $\nu_1 + \nu_{10}$, 1371 cm^{-1}, ν_6), germyl (Ge_2H_5: 767 cm^{-1}, ν_6), digermene (Ge_2H_4: 849 cm^{-1}, ν_{11}), and digermenyl (Ge_2H_3: 1829 cm^{-1}, ν_3) (Fig. 3). The germane-rich nature of the ices was the likely cause that the ethyl (C_2H_5) and vinyl radicals (C_2H_3) were not detected. The pristine ices depict also regions, which are free of absorptions from the reactants and from the synthesized C_2H_x and Ge_2H_x species so that the newly formed $GeCH_x$ molecules (x = 1–6) can be searched for. Upon the onset of the irradiation of the ices, prominent absorption features of the well-known methylgermane molecule (H_3GeCH_3) arose at 871 cm^{-1} (ν_{10}), 1244 cm^{-1} (ν_3), and 1431 cm^{-1} (ν_9); the latter could have some contributions from the ν_6 mode of ethane. The ν_{10} mode (deformation mode) is evidence of the presence of the GeH_3 group; likewise, the ν_3 and ν_9 modes can be attributed to the CH_3 group in the methylgermane molecule. These absorptions agree nicely with those from previous experimental studies [27,28]. Other modes overlap with the absorptions from the reactant molecules or from those arising from the C_2H_x and Ge_2H_x species. Due to the positive identification of methylgermane (H_3GeCH_3) and the agreement between the absorptions from earlier and our present experimental studies, we can also utilize the calculated frequencies (Table 1) to gauge the scaling factor. Recall that scaling factors have to be implemented since the calculated frequencies are often larger than the observed frequencies. The scaling factors account for anharmonicity effects that are neglected in the theoretical calculations, an inadequate description of electron correlation, and the use of finite basis sets. The recommended value of the scaling factor is dependent on the level of theory [29] where Irikura et al. [30] have determined these values by comparing observed vibrational frequencies available through the computational chemistry comparison and benchmark database (CCCBDB; http://cccbdb.nist.gov/) with the calculated values at several levels of theory. For example, their results show that at the B3LYP/6-311G(d,p) level of theory, a recommended scaling factor of 0.967 should be used. The error is reported to be 0.02 in each case. In case of methylgermane (H_3GeCH_3), a comparison of the experimental versus the computed frequencies suggests a scaling factor of 0.974 ± 0.004; this scaling factor is in excellent agreement with the recommended one. Note that an exposure of the D4-methane – D4-germane matrix with energetic electrons also leads to the formation of the perdeuterated form of methylgermane: D_3GeCD_3. Here, absorptions were monitored at 532 cm^{-1} (ν_5), 1463 cm^{-1} (ν_2), and 1479 cm^{-1} (ν_8). Once again, the positions of these absorptions are in excellent agreement with previous studies and – after scaling by 0.978 ± 0.006 – with the computed data.

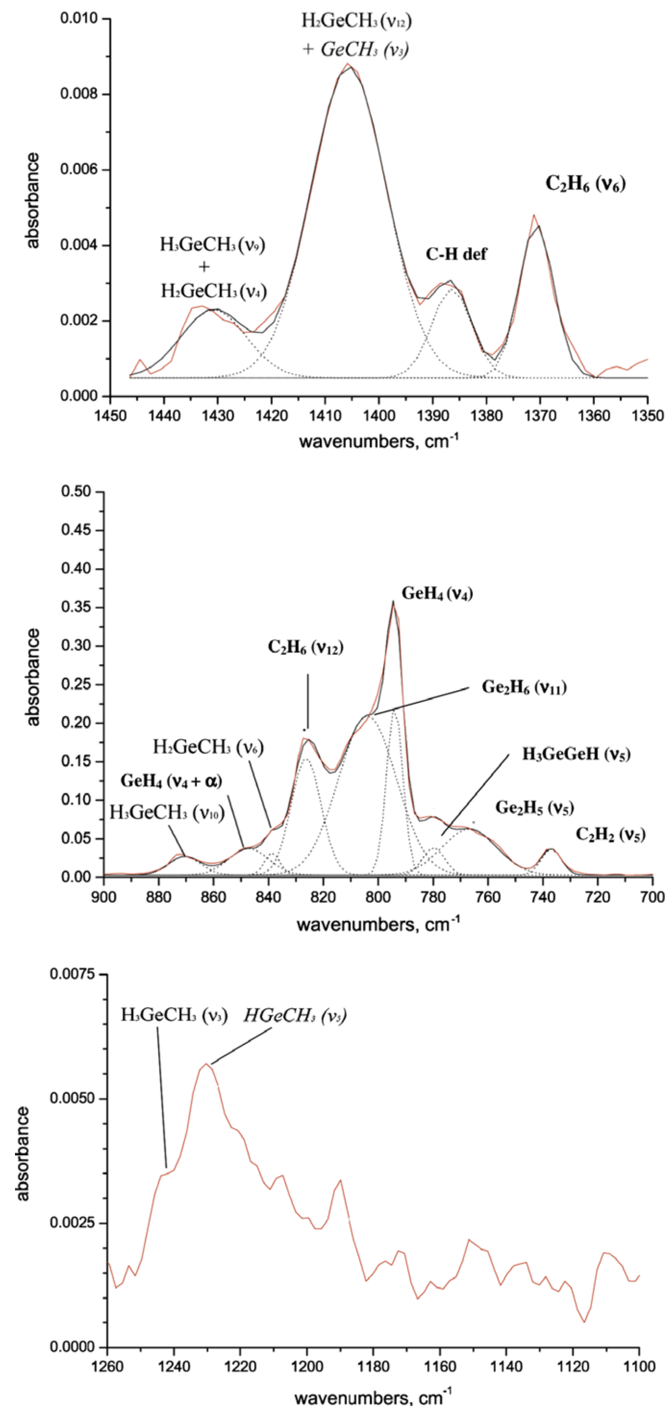

Fig. 3. Absorption features of methylgermane (H_3GeCH_3) and methylgermanyl radicals (H_2GeCH_3) in the irradiated germane – methane ices.

Besides the methylgermane molecule (H_3GeCH_3), we also observed fundamentals which could be attributed to the methylgermyl radical (H_2GeCH_3): the ν_6 mode at 839 cm^{-1} and the ν_{12} absorption at 1406 cm^{-1}; note that the 1431 cm^{-1} absorption could arise from both the methylgermane *and* the methylgermyl radical. Here, the ν_6 mode origins from the GeH_2 scissor, whereas the 1406 cm^{-1} and 1431 cm^{-1} absorptions are evidence of a CH_3 group in the newly formed molecule. Once again, a scaling factor

Table 4
Germanium-carbon-bearing species and their infrared absorptions observed in irradiated methane – germane and D4-methane – D4-germane matrices at 10 K. The identification of the species in italics must be regarded as tentatively.

Species	Frequency, cm^{-1}	Fundamental	Frequency, cm^{-1}	Fundamental	Species
H_3GeCH_3	871	ν_{10}	532	ν_5	D_3GeCD_3
H_3GeCH_3	1244 (sh)	ν_3	1463	ν_2	D_3GeCD_3
H_3GeCH_3	1431	ν_9	1479	ν_8	D_3GeCD_3
H_2GeCH_3	839	ν_6	624	ν_7	D_2GeCD_3
	1406	ν_{12}	1406	ν_3	D_2GeCD_3
	1431	ν_4			
$HGeCH_3$	*1230*	ν_5			
$HGeCH_3$	*1803*	ν_3			
$GeCH_3$	*536*	ν_9			
$GeCH_3$	*1406*	ν_3			

of 0.973 ± 0.005 brings an excellent agreement of the computed with the experimentally observed absorptions. To confirm the formation of the methylgermyl radical, we also inspected the irradiated D4-germane – D4-methane targets. Here, absorptions at 624 cm^{-1} (ν_7) and 1406 cm^{-1} (ν_3) origin from the CD_3 and GeD_2 groups of the D5-methylgermyl radical. Note that we did not observe any absorptions of the thermodynamically less stable H_3GeCH_2 isomer.

In addition to the absorptions as discussed above, we also monitored new features at 1230 cm^{-1}, 1803 cm^{-1}, 1406 cm^{-1}, and 536 cm^{-1} (Table 4, Fig. 3). The first two bands agree nicely – after scaling – with the ν_5 and ν_3 fundamentals of the $HGeCH_3$ molecule. The 536 cm^{-1} and 1406 cm^{-1} peak could be associated with the ν_9 and ν_3 fundamentals of the $GeCH_3$ molecule. However, a look at the irradiated D4-germane – D4-methane target did not depict any absorptions of the perdeuterated $DGeCD_3$ and $GeCD_3$ molecules; the majority of the absorptions are either too weak or overlapped with the reactants or other product molecules. Therefore, the identification of the $HGeCH_3$ and $GeCH_3$ molecules – the thermodynamically most stable isomers of these series – must be regarded as tentatively; this requires further confirmation.

6. Discussion and summary

The observation of the ethane (C_2H_6), digermane (Ge_2H_6), and methylgermane (H_3GeCH_3) molecules suggest that the response of the irradiated ices is dictated by an electron-triggered unimolecular decomposition of the germane (GeH_4) and methane (CH_4) molecules to form the germyl (GeH_3) and methyl radicals (CH_3), respectively, plus atomic hydrogen, reactions (1) and (2), respectively. Two neighboring germyl or methyl radicals could recombine to form digermane or ethane, respectively, in a similar way as established during the irradiation of pure germane [15,16] and methane [12] matrix with energetic electrons as studied earlier in our group. Note that the digermane and ethane molecules are initially internally excited as denoted in Eqs. (3) and (4) by a '*' but can transfer its excess energy to the surrounding matrix to be stabilized. In analogy, the observed methylgermane molecule (H_3GeCH_3) can be formed by recombination of a neighboring germyl radical with a methyl radical (Eq. (5)) via an internally excited methylgermane species.

$$GeH_4 \rightarrow GeH_3 + H \quad (1)$$
$$CH_4 \rightarrow CH_3 + H \quad (2)$$
$$2\ GeH_3 \rightarrow [Ge_2H_6]^* \rightarrow Ge_2H_6 \quad (3)$$
$$2\ CH_3 \rightarrow [C_2H_6]^* \rightarrow C_2H_6 \quad (4)$$
$$GeH_3 + CH_3 \rightarrow [H_3GeCH_3]^* \rightarrow H_3GeCH_3 \quad (5)$$
$$[H_3GeCH_3]^* \rightarrow H_2GeCH_3 + H. \quad (6)$$

What are likely reaction pathways to the newly observed methylgermyl radical (H_2GeCH_3)? First, it is feasible that suprathermal hydrogen atoms, which are generated with a few eV kinetic excess energy in reactions (1) and (2), can abstract a hydrogen atom from the GeH_3 group of methylgermane (H_3GeCH_3) [31,32]. A unimolecular decomposition of the stabilized methylgermane molecule by energetic electrons can also yield the methylgermyl radical via atomic hydrogen elimination. Alternatively, a unimolecular decomposition of *internally excited* methylgermane could result in a germanium – hydrogen bond rupture to form the methylgermyl radical (H_2GeCH_3) via reaction (6). Note that a unimolecular decomposition of *internally excited* ethane and digermane were found to lead to the formation of the ethyl [12] and digermyl radicals [15], respectively. How can we discriminate if the methylgermyl radical (H_2GeCH_3) is formed via unimolecular decomposition of *internally excited* methylgermane, via the hydrogen abstraction, or via radiolysis of stabilized methylgermane? Both latter pathways should form the methylgermyl radical (H_2GeCH_3) radical via higher order kinetic reaction schemes; on the other hand, the unimolecular decomposition of *internally excited* methylgermane should be reflected in a (pseudo) first order kinetics of the methylgermane concentration profile. Here, a kinetic fit of the temporal evolution of the methylgermane molecules, N, could be fit with (pseudo) first order kinetics, i.e. $N = N_0\ (1 - e^{-(kt)})$, with $N_0 = 0.9 \pm 0.1$ and $k = 7.3 \pm 1.9 \times 10^{-4}\ s^{-1}$

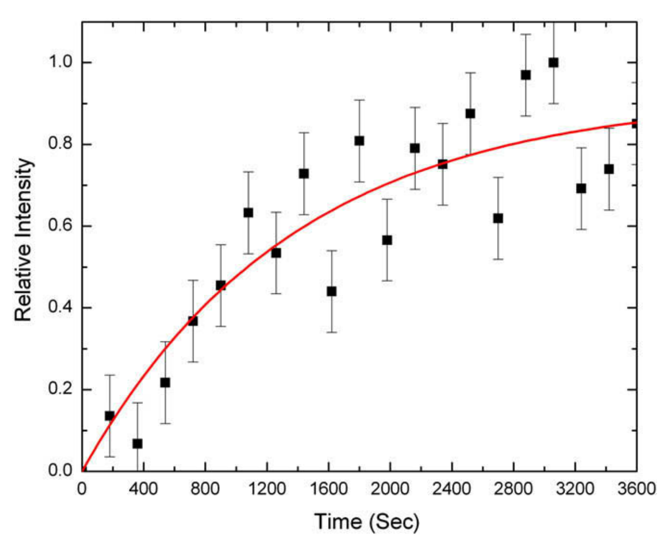

Fig. 4. Temporal evolution of the newly synthesized methylgermyl radical (H_2GeCH_3). The black circles are the data points with error bars, whereas the red solid line presents the best kinetic fit utilizing (pseudo) first order kinetics (see text for discussion). (For interpretation of the references to colour in this figure legend, the reader is referred to the web version of this article.)

(Fig. 4). In summary, we can conclude, that the newly observed methylgermyl radical (H_2GeCH_3) is likely formed via unimolecular decomposition of internally excited methylgermane molecules, which in turn were synthesized as a recombination product of germyl and methyl radicals in the 10 K matrix during the irradiation.

Acknowledgements

The experiments were supported by the NASA Space Grant administered by the University of Hawaii at Manoa (RIK, WC). RMM thanks King Saud University for financial support. Special thanks to Dr. C. Bennett (University of Hawaii) for preparing some of the figures and Dr. F. Zhang (University of Hawaii) for assistance with the references.

References

[1] M. Ueno, Y. Saitoh, Method of producing group III–V compound semiconductor by MOCVD capable of achieving a reduced n-type carrier density, Schottky barrier diode, light emitting diode, laser diode, and method of fabricating the diodes, Application: EP, Sumitomo Electric Industries, Ltd., Japan, 2008, p. 22.
[2] Y. Yashiki, S. Kouketsu, S. Miyajima, A. Yamada, M. Konagai, J. Non-Cryst. Solids 354 (2008) 2355.
[3] Y. Yashiki, S. Kouketsu, S. Miyajima, A. Yamada, M. Konagai, Mater. Res. Soc. Symp. Proc. 989 (2007) 81.
[4] Y.Y. Fang, J. Tolle, J. Tice, A.V.G. Chizmeshya, J. Kouvetakis, V.R. D'Costa, J. Menendez, Chem. Mater. 19 (2007) 5910.
[5] A.B. Chakravarti, A. Dube, R. Loesing, D.J. Schepis, Intermediate-temperature epitaxial growth of Ge-doped carbon–silicon solid solution films on Si during fabrication of N-doped field effect transistors, Application: US, International Business Machines Corporation, USA, 2009, p. 10.
[6] R. Becerra et al., J. Phys. Chem. A 112 (2008) 849.
[7] Y. Yashiki, S. Miyajima, A. Yamada, M. Konagai, Thin Solid Films 501 (2006) 202.
[8] S. Miyajima, Y. Yashiki, A. Yamada, M. Konagai, Thin Solid Films 516 (2008) 670.
[9] J. Dzarnoski, H.E. O'Neal, M.A. Ring, J. Am. Chem. Soc. 103 (1981) 5740.
[10] L. Operti, M. Splendore, G.A. Vaglio, P. Volpe, Organometallics 12 (1993) 4516.
[11] P.v.R. Schleyer, M. Kaupp, F. Hampel, M. Bremer, K. Mislow, J. Am. Chem. Soc. 114 (1992) 6791.
[12] C.J. Bennett, C.S. Jamieson, Y. Osamura, R.I. Kaiser, Astrophys. J. 653 (2006) 792.
[13] D. Sillars, C.J. Bennett, Y. Osamura, R.I. Kaiser, Chem. Phys. 305 (2004) 141.
[14] D. Sillars, C.J. Bennett, Y. Osamura, R.I. Kaiser, Chem. Phys. Lett. 392 (2004) 541.
[15] W. Carrier, W. Zheng, Y. Osamura, R.I. Kaiser, Chem. Phys. 325 (2006) 499.
[16] W. Carrier, W. Zheng, Y. Osamura, R.I. Kaiser, Chem. Phys. 330 (2006) 275.
[17] D.S. Sillars, C.J. Bennett, Y. Osamura, R.I. Kaiser, Chem. Phys. 315 (2005) 41.
[18] C.J. Bennett, D. Sillars, Y. Osamura, R.I. Kaiser, Chem. Phys. Lett. 404 (2005) 327.
[19] C.S. Jamieson, A.M. Mebel, R.I. Kaiser, Chem. Phys. Lett. 440 (2007) 105.
[20] A.D. Becke, J. Chem. Phys. 98 (1993) 5648.
[21] C. Lee, W. Yang, R.G. Parr, Phys. Rev. B: Condens. Matter Mater. Phys. 37 (1988) 785.
[22] R. Krishnan, J.S. Binkley, R. Seeger, J.A. Pople, J. Chem. Phys. 72 (1980) 650.
[23] J. Cizek, Adv. Chem. Phys. 14 (1969) 35.
[24] J.A. Pople, M. Head-Gordon, K. Raghavachari, J. Chem. Phys. 87 (1987) 5968.
[25] R.A. Kendall, T.H. Dunning Jr., R.J. Harrison, J. Chem. Phys. 96 (1992) 6796.
[26] M.J. Frisch et al., Gaussian 98, Revision A11, Gaussian, Inc., Pittsburgh PA, 2002.
[27] J.E. Griffiths, J. Chem. Phys. 38 (1963) 2879.
[28] I.A. Oxton, J. Mol. Struct. 56 (1979) 57.
[29] A.P. Scott, L. Radom, J. Phys. Chem. 100 (1996) 16502.
[30] K.K. Irikura, R.D. Johnson III, R.N. Kacker, J. Phys. Chem. A 109 (2005) 8430.
[31] Q. Zhang, D. Zhang, S. Wang, Y. Gu, J. Phys. Chem. A 106 (2002) 122.
[32] Y.D. Orlov, G. Bouchoux, V.V. Takhistov, D.A. Ponomarev, J. Mol. Struct. 608 (2002) 109.